Inorganic Chemistry

Article

pubs.acs.org/IC

Pressure-Induced Phase Transitions and Correlation between Structure and Superconductivity in Iron-Based Superconductor $Ce(O_{0.84}F_{0.16})FeAs$

Jinggeng Zhao,*[,†,‡] Haozhe Liu,*[,†] Lars Ehm,[‡,§] Dawei Dong,[∥,‡] Zhiqiang Chen,[§] Qingqing Liu,[⊥] Wanzheng Hu,[⊥] Nanlin Wang,[⊥] and Changqing Jin[⊥]

[†]Natural Science Research Center, Academy of Fundamental and Interdisciplinary Sciences, Harbin Institute of Technology, Harbin 150080, China

[‡]Photon Sciences Directorate, Brookhaven National Laboratory, Upton, New York 11973, United States

[§]Mineral Physics Institute, Stony Brook University, Stony Brook, New York 11794, United States

[∥]Department of Physics, Harbin Institute of Technology, Harbin 150080, China

[⊥]Institute of Physics, Chinese Academy of Sciences, Beijing 100190, China

Supporting Information

ABSTRACT: High-pressure angle-dispersive X-ray diffraction experiments on iron-based superconductor $Ce(O_{0.84}F_{0.16})FeAs$ were performed up to 54.9 GPa at room temperature. A tetragonal to tetragonal isostructural phase transition starts at about 13.9 GPa, and a new high-pressure phase has been found above 33.8 GPa. At pressures above 19.9 GPa, $Ce(O_{0.84}F_{0.16})$-FeAs completely transforms to a high-pressure tetragonal phase, which remains in the same tetragonal structure with a larger *a*-axis and smaller *c*-axis than those of the low-pressure tetragonal phase. The structure analysis shows a discontinuity in the pressure dependences of the Fe−As and Ce−(O, F) bond distances, as well as the As−Fe−As and Ce−(O, F)−Ce bond angles in the transition region, which correlates with the change in T_c of this compound upon compression. The isostructural phase transition in $Ce(O_{0.84}F_{0.16})FeAs$ leads to a drastic drop in the superconducting transition temperature T_c and restricts the superconductivity at low temperature. For the 1111-type iron-based superconductors, the structure evolution and following superconductivity changes under compression are related to the radius of lanthanide cations in the charge reservoir layer.

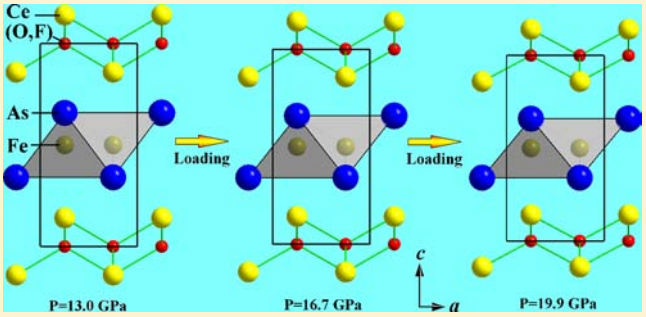

INTRODUCTION

In 2008, superconductivity was found in $La(O_{1-x}F_x)FeAs$ (x = 0.05−0.12), creating a new type of iron-based superconductors.[1] Following the initial discovery, several families of iron-based superconductors have been found, including 1111-type $Ln(O_{1-x}F_x)FeAs$ (Ln = lanthanide elements),[2−5] 122-type $A_{1-x}K_xFe_2As_2$ (A = Ca, Sr, and Ba),[6,7] 111-type Li_xFeAs,[8−10] and 11-type $FeTe_{1-x}Se_x$.[11−14] All these compounds adopt a tetragonal layered structure, with the important Fe−As (or Fe−Te/Se) tetrahedron as the conduction layer. Pressure can effectively adjust the structure and consequent superconductivity in these iron-based superconductors and related precursors.[15−31] Pressure-induced isostructural phase transitions were previously observed in 1111-type $Nd(O_{0.88}F_{0.12})$-FeAs,[15] 122-type $CaFe_2As_2$,[18] $BaFe_2As_2$,[20] $EuFe_2As_2$,[21] and 111-type $Na_{1-x}FeAs$,[22] which seems to be general in these compounds . However, no structural phase transitions have been reported in $La(O_{0.90}F_{0.10})FeAs$ up to about 32 GPa, although it adopts a similar crystal structure with $Nd(O_{1-x}F_x)$-FeAs.[17] The reason for the obvious difference in the structure evolution under high pressure in the 1111-type iron-based superconductor family has to be related sensitively to their crystal structures.

As a 1111-type compound, the superconductivity in $Ce(O_{1-x}F_x)FeAs$ was found with the maximal transition temperatures T_c of about 41 K at x = 0.16.[4] Figure 1 shows the schematic view of crystal structure of $Ce(O_{1-x}F_x)FeAs$ under ambient conditions, in which the As−Fe−As (α and β) and Ce−(O, F)−Ce (γ and δ) angles are highlighted. The T_c of $Ce(O_{1-x}F_x)FeAs$ decreases with pressure and then drops to 0 K, with a drastic drop at about 10−18 GPa for different F content x, obtained from electrical resistance measurements under high pressure.[24,25] For the isostructural F-doped LaOFeAs, the T_c increases with pressure and reaches a maximum of about 43 K at 4 GPa, followed by an

Received: March 25, 2013
Published: July 1, 2013

   dx.doi.org/10.1021/ic400727g | *Inorg. Chem.* 2013, 52, 8067−8073

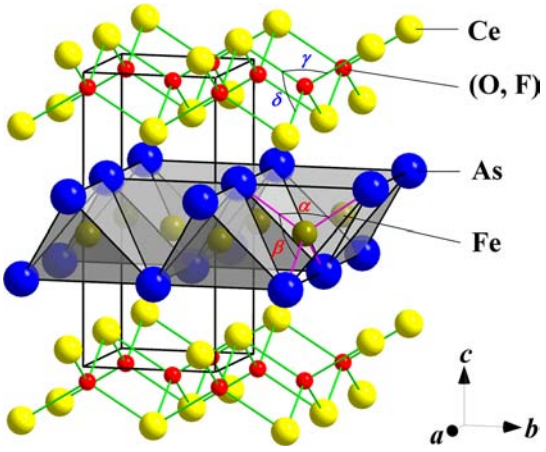

Figure 1. Schematic views of crystal structure of $Ce(O_{0.84}F_{0.16})FeAs$ under ambient conditions.

approximately linear pressure dependence up to about 32 GPa.[23] The obvious difference between these similar compounds shows that further high-pressure structure investigations are important to determine a detailed mechanism of phase transition and gain insight into the pressure effect on the superconductivity correlated with their detailed structures. According to recent neutron scattering investigations, no crystal structural phase transitions have been found when cooling to low temperature in $Ce(O_{1-x}F_x)FeAs$ samples at F-doping $x > 0.10$.[32] So the pressure-induced structure evolution measured at room temperature could elucidate the superconductivity change upon compression at low temperature .

In this work, by using a diamond anvil cell (DAC) technique combined with an in situ angle-dispersive synchrotron X-ray diffraction (AD-XRD) experimental technique, the detailed mechanism of pressure-induced isostructural phase transition on iron-based superconductor $Ce(O_{0.84}F_{0.16})FeAs$ at 13.9 GPa is presented, and a new phase above 33.8 GPa is discovered. The correlation between the pressure dependences of detailed structure evolution and superconductor transition temperature T_c is proposed. The relationship of lanthanide cations radius in the charge reservoir layer and the structure and superconductivity evolution under compression for these 1111-type iron-based superconductors is concluded.

EXPERIMENTAL SECTION

The $Ce(O_{1-x}F_x)FeAs$ samples were synthesized by a solid-state reaction method using CeAs, CeF_3, Fe, FeAs, Fe_2As, and Fe_2O_3 as starting materials.[4] The X-ray diffraction (XRD) pattern indicates that the synthesis yielded an almost pure phase. The in situ high-pressure AD-XRD experiments on $Ce(O_{0.84}F_{0.16})FeAs$ were carried out at room temperature at the beamline X17C of the National Synchrotron Light Source (NSLS), Brookhaven National Laboratory. The incident X-ray monochromatic beam was focused by K−B mirrors to the sample location with the spot size of about 25 × 25 μm^2, with the wavelength of 0.04085 nm. The diameter of flat culets of the diamonds in the diamond anvil cell was 500 or 300 μm. The sample was prepressed to a pellet with thickness about 10−15 μm, and then loaded into the sample chamber of 120−160 μm diameter which was drilled in the T301 stainless steel gasket and preindented to 40−55 μm thickness. This could avoid sample bridging with anvils during compression.

The pressure was measured by using the ruby luminescence method with the laser wavelength of 532.1 nm.[33] Silicone oil were used as the pressure-transmitting medium, which ensured a quasi-hydrostatic pressure environment within the experimental pressure range.[34,35] Two-dimensional diffraction patterns were collected on a charge-coupled device (CCD) detector with the typical exposure time of 1200 s. The distance between sample and detector and the orientation parameters of the detector were calibrated using CeO_2 standard. The recorded images were integrated using the program Fit2D.[36] The XRD patterns under high pressure were analyzed with Rietveld refinements by using the GSAS program package.[37,38]

RESULTS AND DISCUSSION

Figure 2 shows the selected X-ray diffraction patterns of $Ce(O_{0.84}F_{0.16})FeAs$ up to 54.9 GPa at room temperature. In the

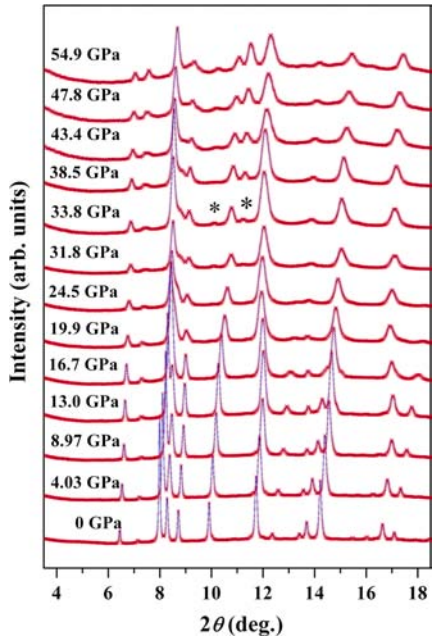

Figure 2. Spectra of angle-dispersive X-ray diffraction patterns of $Ce(O_{0.84}F_{0.16})FeAs$ at room temperature up to 54.9 GPa (λ = 0.04085 nm). The asterisk in the XRD pattern indicates the diffraction peaks from the new structure at about 33.8 GPa.

pressure range of 0−31.8 GPa, no new peaks are observed. However, the shift of position of several peaks with pressure is abnormal at pressure above 13.9 GPa. Figure 3 shows the detail change of peak (112) and (200) for $Ce(O_{0.84}F_{0.16})FeAs$ in the pressure range of 10.5−21.7 GPa. The bold lines in Figure 3, guided for the eyes, indicate that the peak (200) starts to shift to low-angle direction with increasing pressure from 13.9 GPa, and then moves to normal high-angle direction after 19.9 GPa. The peak (112) shifts to high-angle direction in this pressure region. Figure 4 shows the relationships of d spacing and full width at half-maximum (FWHM) of peak (112) and (200) versus pressure. With increasing pressure, d_{112} decreases, but d_{200} first increases from 13.9 to 19.1 GPa, and then decreases above 19.9 GPa. The FWHM of the two peaks increases with pressure below 19.1 GPa, and decreases above 19.9 GPa. According to the pressure dependences of d spacing and FWHM of these two peaks, the structural phase transition can be found from 13.9 GPa and finishes after 19.9 GPa.

At about 33.8 GPa, the emergence of two new weak diffraction peaks at 2θ of about 10.1° and 11.3°, indicated by the asterisk in the XRD pattern in Figure 2, shows that $Ce(O_{0.84}F_{0.16})FeAs$ transforms to a new high-pressure phase. With increasing pressure, the intensity of these two peaks increases. Up to the maximal pressure of 54.9 GPa, the original phase still remains as the main content in the XRD pattern, so

dx.doi.org/10.1021/ic400727g | Inorg. Chem. 2013, 52, 8067−8073

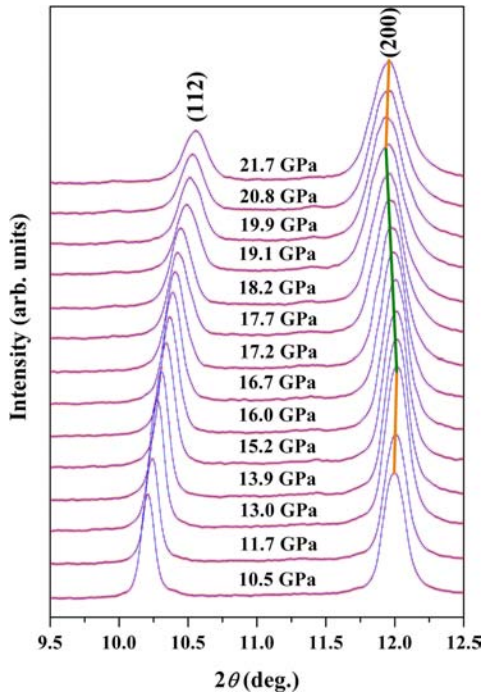

Figure 3. Details of peak (112) and (200) of $Ce(O_{0.84}F_{0.16})FeAs$ in the range of 10.5−21.7 GPa (λ = 0.04085 nm).

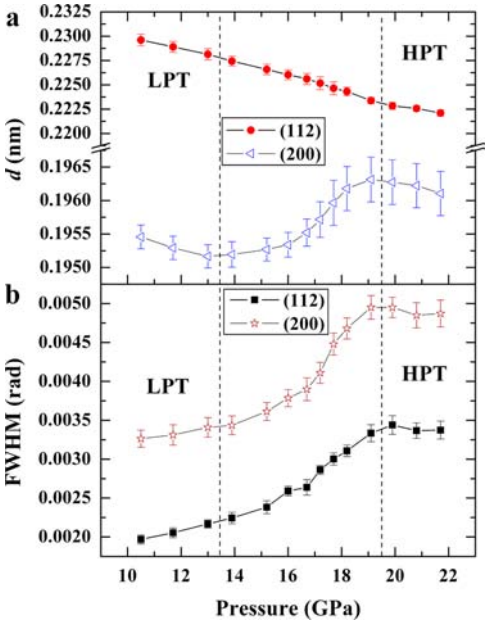

Figure 4. Pressure dependences of (a) *d* spacing and (b) full width at half-maximum (FWHM) of peak (112) and (200) of $Ce(O_{0.84}F_{0.16})$-FeAs in the pressure range of 10.5−21.7 GPa.

the two phases coexist in a large pressure region. It is difficult to index the crystal structure of this new phase, since only two new diffraction peaks were found in the XRD patterns. $Ce(O_{0.84}F_{0.16})FeAs$ recovers to the original structure at pressure release, which shows that the phase transition is fully reversible. The similar pressure-induced new phase has been also observed in the 111-type iron-based superconductor $Na_{1-x}FeAs$ above about 20 GPa.[22]

Figure 5a shows the evolution of unit cell parameters of $Ce(O_{0.84}F_{0.16})FeAs$ in the pressure range of 0−31.8 GPa, which

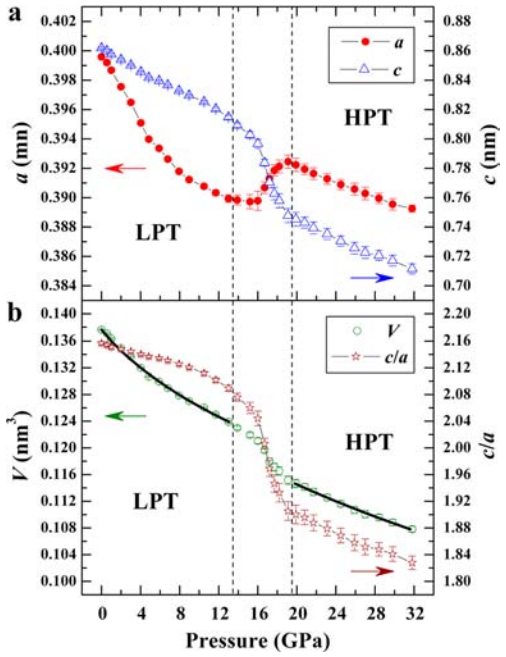

Figure 5. Pressure dependences of (a) lattice parameters and (b) unit cell volume and the *c*/*a* ratio of $Ce(O_{0.84}F_{0.16})FeAs$ up to 31.8 GPa. The solid lines in (b) are the fitting results according to the Birch equation of state (EoS).

were determined from Le Bail refinements based on previous reported unit cell.[4] Below 13.0 GPa, both the *a*- and *c*-axis shrink with increasing pressure. From 13.9 GPa, the value of *a*-axis decreases slowly with pressure, and then starts to increase between 15.2 and 19.1 GPa. The *c*-axis drastically decreases within the pressure range of 13.9−19.1 GPa. At pressures above 19.9 GPa, both the *a* and *c* axis decrease up to the maximal experimental pressure. These results show an isostructural phase transition starting at about 13.9 GPa. Above 19.9 GPa, $Ce(O_{0.84}F_{0.16})FeAs$ transforms completely to a high-pressure tetragonal (HPT) structure keeping the same space group of *P*4/*nmm* but with a lager *a*-axis and smaller *c*-axis, compared to the primary low-pressure tetragonal (LPT) structure. The schematic view of structure evolution with pressure in the transition region of $Ce(O_{0.84}F_{0.16})FeAs$ is shown in the Table of Contents. The pressure dependence of the *c*/*a* ratio is presented in Figure 5b, showing a drastic drop between 13.9 and 19.1 GPa.

Figure 5b also shows the pressure dependence of unit cell volume for $Ce(O_{0.84}F_{0.16})FeAs$, where the solid lines are the fitting results for the LPT and HPT phases, by using the Birch equation of state (EoS).[39] We obtained the ambient pressure isothermal bulk modulus B_0 = 94(2) GPa with B_0' of 5, and B_0 = 98(3) GPa with B_0' of 4, for the LPT and HPT phases, respectively. The fitted unit cell volume V_0 of the two phases at ambient conditions is equal to 0.1375(2) and 0.1332(6) nm^3, respectively. The B_0 of the LPT phase of $Ce(O_{0.84}F_{0.16})FeAs$ is smaller than that of $Nd(O_{0.88}F_{0.12})FeAs$ (102(2) GPa),[15] and $Sm(O_{0.93}F_{0.07})FeAs$ (103(1) GPa),[16] and is larger than that of $La(O_{0.9}F_{0.1})FeAs$ (78(2) GPa).[17] The range of 13.0−19.9 GPa is a transitional region between the LPT and HPT phases, with a discontinued variation in the *V*-*P* curve.

The structure of $Ce(O_{0.84}F_{0.16})FeAs$ below 24.5 GPa was refined from the XRD patterns by using the Rietveld method, to study the pressure effect on the structural properties down to

dx.doi.org/10.1021/ic400727g | Inorg. Chem. 2013, 52, 8067−8073

the atomic level. The typical refinement results at 4.03 and 17.7 GPa are shown in Figure 6, with the R_{wp} factor of 5.13% and

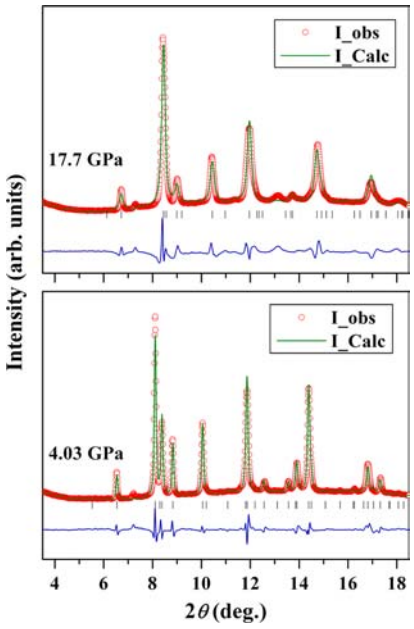

Figure 6. Experimental (open circle) and fitted (line) X-ray diffraction patterns for $Ce(O_{0.84}F_{0.16})FeAs$ at 4.03 and 17.7 GPa (λ = 0.04085 nm). The vertical lines are denoted the Bragg peaks in the XRD patterns.

6.32%, respectively. The pressure dependences of the atomic parameter z of As and Ce ions of $Ce(O_{0.84}F_{0.16})FeAs$ are shown in the Supporting Information, Figure S1. Changes in the atomic parameters under compression are only small within the experimental errors, except in the transition region from the LPT to HPT phases, that is, the region of 13.0−19.9 GPa. Figure 7 shows the pressure dependences of selected bond

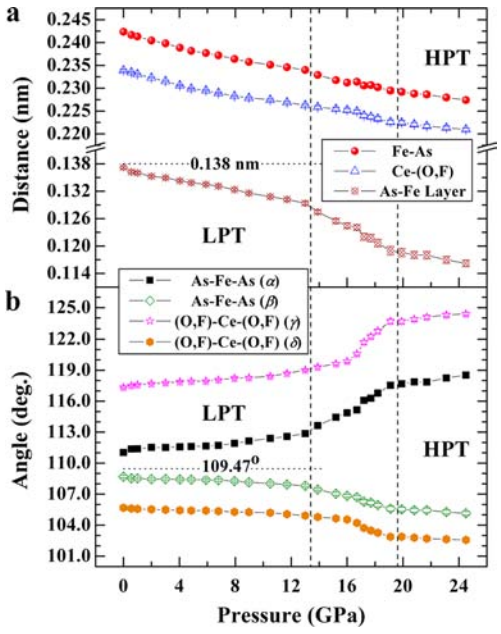

Figure 7. Pressure dependences of (a) bond distances and As anion height from Fe layer, and (b) bond angles for $Ce(O_{0.84}F_{0.16})FeAs$ up to 24.5 GPa. The angle $\alpha-\delta$ is indicated in Figure 1.

distances and angles, in which the angle $\alpha-\delta$ is indicated in Figure 1, as well as the As anion height, that is, the distance between the As anion and Fe layer. Both the As anion height and the Fe−As and Ce−(O, F) distances decrease with increasing pressure, with the discontinuity transition in the pressure region of 13.9−19.1 GPa. At ambient pressure, both the As−Fe−As angle α of 111.0(1)° (×2) and β of 108.7(1)° (×4) are close to 109.47°, which indicates that the $FeAs_4$ tetrahedron can be regarded as a regular one. The Ce−(O, F)−Ce angle γ of 117.34(9)° (×2) and δ of 105.68(9)° (×4) show that the (O, F)Ce_4 tetrahedron is distorted at ambient pressure. With increasing pressure, the As−Fe−As angle β and Ce−(O, F)−Ce angle δ are decreasing, with a drastic drop in the transition region of 13.9−19.1 GPa. The pressure dependences of α and γ angles are reversed with those of β and δ angles.

The superconductivity for most iron-based superconductors is closely related to their detailed structure. The T_c seem to gain maximal values when the As−Fe−As angles are equal to 109.47°,[40] or the As anion height is equal to 0.138 nm obtained by theoretical and experimental works.[41,42] Figure 8a combines

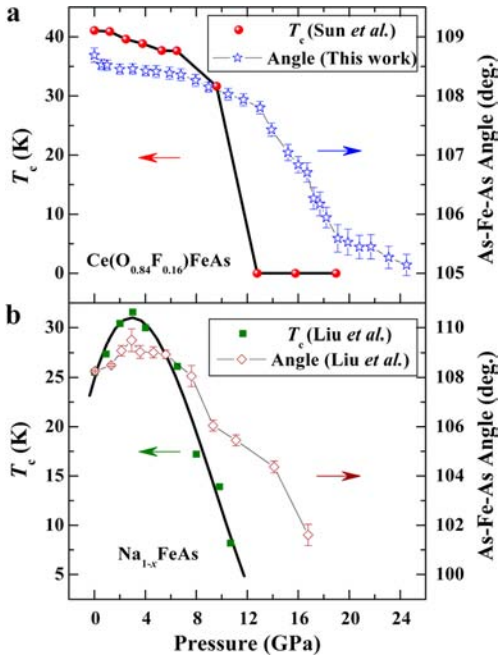

Figure 8. Pressure dependences of T_c and As−Fe−As angle (β) for (a) $Ce(O_{0.84}F_{0.16})FeAs$ and (b) $Na_{1-x}FeAs$. The results of T_c for $Ce(O_{0.84}F_{0.16})FeAs$ and T_c and As−Fe−As angle for $Na_{1-x}FeAs$ are obtained from refs 24 and 22, respectively.

the pressure dependences of T_c and As−Fe−As angle(β) for $Ce(O_{0.84}F_{0.16})FeAs$, in which the data of T_c are obtained from ref 24. The trends in the pressure-induced decrease of T_c and As−Fe−As angle(β) are similar to each other before the tetragonal to tetragonal isostructural phase transition. In the transition process from LPT to HPT phase, the drastic drop in the angle(β)-P curve shows the increasing distortion degree of the $FeAs_4$ tetrahedron. Accordingly, the T_c decreases drastically with pressure as well, and then drops to 0 K at about 12.8 GPa.[24] The phase transition pressure normally will decrease under nonhydrostatic conditions compared to quasi-hydrostatic conditions.[43] In the electrical resistance measurements under pressure in ref 24, the solid pressure-transmitting medium may induce the lower transition pressure than that in the liquid

dx.doi.org/10.1021/ic400727g | Inorg. Chem. 2013, 52, 8067−8073

medium in the structural experiments in this work. In other words, the different pressure-transmitting medium in the electrical properties and structure measurements induced the different transition pressure between T_c−P and β−P curves. Thus the pressure at T_c = 0 K in ref 24 may be corresponding to that when the isostructural phase transition has finished in this work. The analogous case exists in 111-type iron-based superconductor $Na_{1-x}FeAs$.[22] The relationships of T_c and As−Fe−As angle of $Na_{1-x}FeAs$ are shown in Figure 8b as a comparison to $Ce(O_{0.84}F_{0.16})FeAs$.[22] After the isostructural phase transition, the As−Fe−As angle β of $Ce(O_{0.84}F_{0.16})FeAs$ is smaller than 105.53°, and α is larger than 117.68°, which corresponds to the T_c = 0 K case.[40] On the other hand, the value of 0.1372(3) nm for the As anion height at ambient pressure in $Ce(O_{0.84}F_{0.16})FeAs$ is smaller than 0.138 nm. The As anion height decreases with increasing pressure and shifts to the lower value direction from 0.138 nm, which is consistent with the decrease of T_c under compression. After the isostructural phase transition, the As anion height is smaller than 0.118 nm, which corresponds to the T_c = 0 K case.[41,42] Therefore, according to the pressure dependences of As−Fe−As angles and As anion height from the Fe layer, the isostructural phase transition in $Ce(O_{0.84}F_{0.16})FeAs$ under compression results in the drastic drop of T_c, and eventually the high-pressure tetragonal phase loses the superconductivity at low temperature.

The ion size plays an important role in the superconductivity and structure evolution under pressure in the iron-based superconductors. For example, in the 1111-type RE-$Fe_{0.85}Ir_{0.15}AsO$ (RE = La, Nd, Sm, and Gd) system, T_c increases with decreasing lanthanide cation size from La to Gd.[44] So the cation effects are an important factor that should be considered in the research on the iron-based superconductors. The 1111-type iron-based superconductors $Ln(O_{1-x}F_x)FeAs$ (Ln = La, Ce, Pr, Nd, and Sm) have different pressure dependences of structure and superconductivity with each other,[15−17,23−26] because of the different lanthanide cation radius in the $Ln_2(O, F)_2$ charger reservoir layer. Their corresponding high pressure experimental results are summarized in the Supporting Information, Table S1. For the $La(O_{1-x}F_x)FeAs$ series, no structural phase transitions happen up to about 32 GPa at x = 0.10,[17] and T_c decreases linearly with pressure after obtaining its maximum at about 4 GPa for the x = 0.11 sample,[21] without the drastic drop in the T_c−P curve. Similar results exist in Sm-based compounds.[24] However, in the sister compounds $Ce(O_{1-x}F_x)FeAs$ and $Nd(O_{1-x}F_x)FeAs$, the compression induces them to transform to a collapsed tetragonal structure,[15] as well as the loss of superconductivity after the isostructural phase transition.[24] So there is a correlation between the structure and superconductivity under high pressure for these 1111-type compounds, in which the tetragonal to tetragonal isostructural phase transition corresponds to the drastic variation of the T_c−P curve under compression,[24] and as a comparison, the continued structure evolution corresponds to the linear decrease of T_c with pressure.[17,26]

The shearing movement of the charge reservoir layer during compression is a possible driving force for the isostructural phase transition.[15] In $Ce(O_{1-x}F_x)FeAs$, the $(O, F)Ce_4$ tetrahedron is not stable, because of the close ion radius between Ce^{3+} and O^{2-}/F^-,[45] which is different from the $FeAs_4$ tetrahedron. So the movement of the $Ce_2(O, F)_2$ layer is easier than that of the Fe_2As_2 layer under compression. Recently, theoretical works in $CaFe_2As_2$ and $BaFe_2As_2$ show that the structure phase transitions under hydrostatic pressure are similar with those under uniaxial pressure parallel to the c-axis.[46] This could be a reference to the compression behavior of 1111-type series. The shearing movement of the $Ce_2(O, F)_2$ layer in the ab-plane during compression may result in the enlargement of the a-axis, which is a possible reason for the isostructural phase transition in $Ce(O_{0.84}F_{0.16})FeAs$. For the $Ln(O_{1-x}F_x)FeAs$ series, the size of lanthanide element cations in the charge reservoir layer may induce the dissimilar shearing movement degree under compression. Therefore, no isostructural phase transitions have been found for the compounds including larger or smaller cations in the experimental pressure range, such as the $La(O_{1-x}F_x)FeAs$ and $Sm(O_{1-x}F_x)FeAs$ series.[17,26] The similar pressure behavior related to ion radius exists in ARh_2P_2 (A = Ca, Sr, Ba) with the $TiCr_2Si_2$ structure,[47] that is, the 122-type structure for iron-based superconductors. The $SrRh_2P_2$ undergoes an isostructural phase transition at about 6 GPa, which is different from that in the corresponding Ba and Ca compounds.

CeOFeP, which is isostructural with CeOFeAs, is a heavy fermion system and does not have any superconductivity at low temperature.[48] The isostructural phase transition under high pressure may result in that $Ce(O_{1-x}F_x)FeAs$ series convert to a heavy electron system, since the bandwidth of the valence band in them is close to that of CeOFeP. This is a possible reason for loss of superconductivity in the HPT phase of $Ce(O_{0.84}F_{0.16})$-FeAs. In the 1111-type LnOFeP (Ln = La, Ce, Pr, Nd, Sm) series, the superconductivity exists in LaOFeP and SmOFeP.[49−51] However, the sister compounds CeOFeP, PrOFeP, and NdOFeP remain nonsuperconducting at low temperature.[48,52,53] The annealed PrOFeP and NdOFeP were reported to be superconducting,[51] which may be due to the change of oxygen content. The LnOFeP series including lager or smaller Ln ions (La and Sm) have superconductivity at low temperature, being contrary to the other ones (Ce, Pr, and Nd). For the 1111-type $Ln(O_{1-x}F_x)FeAs$ (Ln = La, Ce, Pr, Nd, Sm) series, there is no isostructural phase transition in the compounds including larger or smaller Ln ions (La and Sm) under compression, being contrary to the other ones (Ce and Nd). Comparing with the two cases in $Ln(O_{1-x}F_x)FeAs$ and LnOFeP series, the effect of Ln ion radius on the structural evolution under compression in the former is similar with that on the superconductivity in the latter. More experimental data on LnOFeP will be helpful to understand the structure and superconductivity evolution under high pressure of these compounds and the $Ln(O_{1-x}F_x)FeAs$ series.

As shown in Supporting Information, Table S1, no structure and superconductivity investigations under high pressure for $Pr(O_{1-x}F_x)FeAs$ compounds have been performed up to date. Since the radius of Pr cation is in the middle of that of Ce and Nd cations,[45] the F-doped PrOFeAs may also come through a similar isostructural phase transition and the drastic drop of T_c-P curve with $Ce(O_{1-x}F_x)FeAs$ and $Nd(O_{1-x}F_x)FeAs$. The corresponding high-pressure structural and physical measurements on $Pr(O_{1-x}F_x)FeAs$ could test the pressure behavior of the $Ln(O_{1-x}F_x)FeAs$ series. Furthermore, as a new unknown structure, the high-pressure phase above 33.8 GPa in $Ce(O_{0.84}F_{0.16})FeAs$ has not been discovered in other 1111-type iron-based superconductors up to now, and may have a new electronic state under compression. So it is necessary to perform further in situ high-pressure experiments on these superconductor materials to obtain more structural and physical

dx.doi.org/10.1021/ic400727g | Inorg. Chem. 2013, 52, 8067−8073

properties of these compounds under higher pressure conditions.

CONCLUSIONS

The tetragonal to tetragonal isostructural phase transition at 13.9 GPa and another high-pressure new phase at 33.8 GPa in the iron-based superconductor $Ce(O_{0.84}F_{0.16})FeAs$ were found by the high-pressure angle-dispersive X-ray diffraction experiments. The results of detailed crystal structure evolution under pressure provide the essential information for the pressure dependence of the superconductor transition temperature T_c. The relationships of T_c versus As−Fe−As bond angle and As anion height upon compression indicate that the pressure-induced isostructural phase transition drastically compresses T_c and results in the loss of superconductivity at low temperature. The pressure dependences of structure and superconductivity of the 1111-type iron-based superconductors are related to the radius of lanthanide element cations in the charge reservoir layer. These high-pressure structural transition behaviors are helpful for us to understand the universal structural evolution pattern in iron-based superconductors upon compression.

ASSOCIATED CONTENT

Supporting Information

The pressure dependences of the atomic parameter z of As and Ce ions of $Ce(O_{0.84}F_{0.16})FeAs$ (Figure S1), and the summary of structure and superconductivity under high pressure for the 1111-type iron-based superconductors $Ln(O_{1-x}F_x)FeAs$ (Ln = La, Ce, Pr, Nd, Sm) (Table S1). This material is available free of charge via the Internet at http://pubs.acs.org.

AUTHOR INFORMATION

Corresponding Author

*E-mail: haozhe@hit.edu.cn (H.L.), zhaojinggeng@gmail.com (J.Z.).

Notes

The authors declare no competing financial interest.

ACKNOWLEDGMENTS

We thank the support from the National Natural Science Foundation of China (Grant Nos. 10904022, 10975042), the China Postdoctoral Science Foundation special funded project (Grant No. 200902410), the Postdoctoral Science-research Developmental Foundation of Heilongjiang Province (Grant No. LBH-Q12095), the Fundamental Research Funds for the Central Universities (Grant No. HIT.NSRIF.2013054), and the program for Basic Research Excellent Talents and Oversea Collaborative Base Project in Harbin Institute of Technology (HIT). The work at IOPCAS was supported by NSF and MOST of China through research projects. We also thank the support from COMPRES (the Consortium for Materials Properties Research in Earth Sciences) and the National Synchrotron Light Source, Brookhaven National Laboratory, supported by the U.S. Department of Energy, Office of Science, Office of Basic Energy Sciences, under Contract No. DE-AC02-98CH10886.

REFERENCES

(1) Kamihara, Y.; Watanabe, T.; Hirano, M.; Hosono, H. *J. Am. Chem. Soc.* **2008**, *130*, 3296−3297.
(2) Chen, X. H.; Wu, T.; Wu, G.; Liu, R. H.; Chen, H.; Fang, D. F. *Nature* **2008**, *453*, 761−762.
(3) Ren, Z.-A.; Yang, J.; Lu, W.; Yi, W.; Shen, X.-L.; Li, Z.-C.; Che, G.-C.; Dong, X.-L.; Sun, L.-L.; Zhou, F.; Zhao, Z. X. *Europhys. Lett.* **2008**, *82*, 57002.
(4) Chen, G. F.; Li, Z.; Wu, D.; Li, G.; Hu, W. Z.; Dong, J.; Zheng, P.; Luo, J. L.; Wang, N. L. *Phys. Rev. Lett.* **2008**, *100*, 247002.
(5) Chen, G. F.; Li, Z.; Wu, D.; Dong, J.; Li, G.; Hu, W. Z.; Zheng, P.; Luo, J. L.; Wang, N. L. *Chin. Phys. Lett.* **2008**, *25*, 2235−2238.
(6) Cheng, P.; Shen, B.; Mu, G.; Zhu, X. Y.; Han, F.; Zeng, B.; Wen, H. H. *Europhys. Lett.* **2009**, *85*, 67003.
(7) Rotter, M.; Tegel, M.; Johrendt, D. *Phys. Rev. Lett.* **2008**, *101*, 107006.
(8) Wang, X. C.; Liu, Q. Q.; Lv, Y. X.; Gao, W. B.; Yang, L. X.; Yu, R. C.; Li, F. Y.; Jin, C. Q. *Solid State Commun.* **2008**, *148*, 538−540.
(9) Pitcher, M. J.; Parker, D. R.; Adamson, P.; Herkelrath, J. C.; Boothroyd, A. T.; Ibberson, R. M.; Brunelli, M.; Clarke, S. J. *Chem. Commun.* **2008**, *45*, 5918−5920.
(10) Tapp, J. H.; Tang, Z.; Lv, B.; Sasmal, K.; Lorenz, B.; Chu, C. W.; Guloy, A. M. *Phys. Rev. B* **2008**, *78*, 060505.
(11) Hsu, F. C.; Luo, J. Y.; Yeh, K. W.; Chen, T. K.; Huang, T. W.; Wu, P. M.; Lee, Y. C.; Huang, Y. L.; Chu, Y. Y.; Yan, D. C.; Wu, M. K. *Proc. Natl. Acad. Sci. U.S.A.* **2008**, *105*, 14262−14264.
(12) Mizuguchi, Y.; Tomioka, F.; Tsuda, S.; Yamaguchi, T.; Takano, Y. *Appl. Phys. Lett.* **2009**, *94*, 012503.
(13) Chen, G. F.; Hu, W. Z.; Luo, J. L.; Wang, N. L. *Phys. Rev. Lett.* **2009**, *102*, 227004.
(14) Parker, D. R.; Pitcher, M. J.; Baker, P. J.; Franke, I.; Lancaster, T.; Blundell, S. J.; Clarke, S. J. *Chem. Commun.* **2009**, *16*, 2189−2191.
(15) Zhao, J. G.; Wang, L. H.; Dong, D. W.; Liu, Z. G.; Liu, H. Z.; Chen, G. F.; Wu, D.; Luo, J. L.; Wang, N. L.; Yu, Y.; Jin, C. Q.; Guo, Q. Z. *J. Am. Chem. Soc.* **2008**, *130*, 13828−13829.
(16) Martinelli, A.; Ferretti, M.; Palenzon, A.; Merlini, M. *Phys. C* **2009**, *469*, 782−784.
(17) Garbarino, G.; Toulemonde, P.; Álvarez-Murga, M.; Sow, A.; Mezouar, M.; Núñez-Regueiro, M. *Phys. Rev. B* **2008**, *78*, 100507(R).
(18) Kreyssig, A.; Green, M. A.; Lee, Y.; Samolyuk, G. D.; Zajdel, P.; Lynn, J. W.; Bud'ko, S. L.; Torikachvili, M. S.; Ni, N.; Nandi, S.; Leão, J. B.; Poulton, S. J.; Argyriou, D. N.; Harmon, B. N.; McQueeney, R. J.; Canfield, P. C.; Goldman, A. I. *Phys. Rev. B* **2008**, *78*, 184517.
(19) Mito, M.; Pitcher, M. J.; Crichton, W.; Garbarino, G.; Baker, P. J.; Blundell, S. J.; Adamson, P.; Parker, D. R.; Clarke, S. J. *J. Am. Chem. Soc.* **2009**, *131*, 2986−2992.
(20) Mittal, R.; Mishra, S. K.; Chaplot, S. L.; Ovsyannikov, S. V.; Greenberg, E.; Trots, D. M.; Dubrovinsky, L.; Su, Y.; Brueckel, Th.; Matsuishi, S.; Hosono, H.; Garbarino, G. *Phys. Rev. B* **2011**, *83*, 054503.
(21) Uhoya, W.; Tsoi, G.; Vohra, Y. K.; McGuire, M. A.; Sefat, A. S.; Sales, B. C.; Mandrus, D.; Weir, S. T. *J. Phys.: Condens. Matter* **2010**, *22*, 292202.
(22) Liu, Q. Q.; Yu, X. H.; Wang, X. C.; Deng, Z.; Lv, Y. X.; Zhu, J. L.; Zhang, S. J.; Liu, H. Z.; Yang, W. G.; Wang, L.; Mao, H. K.; Shen, G. Y.; Lu, Z. Y.; Ren, Y.; Chen, Z. Q.; Lin, Z. J.; Zhao, Y. S.; Jin, C. Q. *J. Am. Chem. Soc.* **2011**, *133*, 7892−7896.
(23) Takahashi, H.; Igawa, K.; Arii, K.; Kamihara, Y.; Hirano, M.; Hosono, H. *Nature* **2008**, *453*, 376−378.
(24) Sun, L. L.; Dai, X.; Zhang, C.; Yi, W.; Chen, G. F.; Wang, N. L.; Zheng, L. R.; Jiang, Z.; Wei, X. J.; Huang, Y. Y.; Wang, J.; Ren, Z. A.; Lu, W.; Dong, X. L.; Che, G. C.; Wu, Q.; Ding, H.; Liu, J.; Hu, T. D.; Zhao, Z. X. *Europhys. Lett.* **2010**, *91*, 57008.
(25) Zocco, D. A.; Hamlin, J. J.; Baumbach, R. E.; Maple, M. B.; McGuire, M. A.; Sefat, A. S.; Sales, B. C.; Lin, R.; Mandrus, D.; Jeffries, J. R.; Weir, S. T.; Vohra, Y. K. *Phys. C* **2008**, *468*, 2229−2232.
(26) Garbarino, G.; Weht, R.; Sow, A.; Sulpice, A.; Toulemonde, P.; Álvarez-Murga, M.; Strobel, P.; Bouvier, P.; Mezouar, M.; Núñez-Regueiro, M. *Phys. Rev. B* **2011**, *84*, 024510.
(27) Igawa, K.; Okada, H.; Takahashi, H.; Matsuishi, S.; Kamihara, Y.; Hirano, M.; Hosono, H.; Matsubayashi, K.; Uwatoko, Y. *J. Phys. Soc. Jpn.* **2009**, *78*, 025001.

(28) Zhang, S. J.; Wang, X. C.; Sammynaiken, R.; Tse, J. S.; Yang, L. X.; Li, Z.; Liu, Q. Q.; Desgreniers, S.; Yao, Y.; Liu, H. Z.; Jin, C. Q. *Phys. Rev. B* **2009**, *80*, 014506.
(29) Gooch, M.; Lv, B.; Tapp, J. H.; Tang, Z.; Lorenz, B.; Guloy, A. M.; Chu, P. C. W. *Europhys. Lett.* **2009**, *85*, 27005.
(30) Mizuguchi, Y.; Tomioka, F.; Tsuda, S.; Yamaguchi, T.; Takano, Y. *Appl. Phys. Lett.* **2008**, *93*, 152505.
(31) Margadonna, S.; Takabayashi, Y.; Ohishi, Y.; Mizuguchi, Y.; Takano, Y.; Kagayama, T.; Nakagawa, T.; Takata, M.; Prassides, K. *Phys. Rev. B* **2009**, *80*, 064506.
(32) Zhao, J.; Huang, Q.; de la Cruz, C.; Li, S. L.; Lynn, J. W.; Chen, Y.; Green, M. A.; Chen, G. F.; Li, G.; Li, Z.; Luo, J. L.; Wang, N. L.; Dai, P. C. *Nat. Mater.* **2008**, *7*, 953−959.
(33) Mao, H. K.; Xu, J. A.; Bell, P. M. *J. Geophys. Res.* **1986**, *91*, 4673−4676.
(34) Shen, Y. R.; Kumar, R. S.; Pravica, M.; Nicol, M. F. *Rev. Sci. Instrum.* **2004**, *75*, 4450−4454.
(35) Liu, H. Z.; Hu, J. Z.; Shu, J. F.; Häusermann, D.; Mao, H.−K. *Appl. Phys. Lett.* **2004**, *85*, 1973−1975.
(36) Hammersley, A. P.; Svensson, S. O.; Hanfland, M.; Fitch, A. N.; Häusermann, D. *High Pressure Res.* **1996**, *14*, 235−248.
(37) Rietveld, H. M. *Acta Crystallogr.* **1967**, *22*, 151−152.
(38) Larson, A. C.; Von Dreele, R. B. *General Structure Analysis System (GSAS)*, Los Alamos National Laboratory, Report LAUR 86-748; Los Alamos National Laboratory: Los Alamos, NM, 1994.
(39) Birch, F. *Phys. Rev.* **1947**, *71*, 809−824.
(40) Lee, C. H.; Iyo, A.; Eisaki, H.; Kito, H.; Fernandez-Diaz, M. T.; Ito, T.; Kihou, K.; Matsuhata, H.; Braden, M.; Yamada, K. *J. Phys. Soc. Jpn.* **2008**, *77*, 083704.
(41) Kuroki, K.; Usui, H.; Onari, S.; Arita, R.; Aoki, H. *Phys. Rev. B* **2009**, *79*, 224511.
(42) Mizuguchi, Y.; Hara, Y.; Deguchi, K.; Tsuda, S.; Yamaguchi, T.; Takeda, K.; Kotegawa, H.; Tou, H.; Takano, Y. *Supercond. Sci. Technol.* **2010**, *23*, 054013.
(43) Uhoya, W.; Stemshorn, A.; Tsoi, G.; Vohra, Y. K.; Sefat, A. S.; Sales, B. C.; Hope, K. M.; Weir, S. T. *Phys. Rev. B* **2010**, *82*, 144118.
(44) Maroni, B.; Castro, D. D.; Hanfland, M.; Boby, J.; Vercesi, C.; Mozzati, M. C.; Weyeneth, S.; Keller, H.; Khasanov, R.; Drathern, C.; Dore, P.; Postorino, P.; Malavasi, L. *J. Am. Chem. Soc.* **2011**, *133*, 3252−3255.
(45) Shannon, R. D. *Acta Crystallogr.* **1976**, *A32*, 751−767.
(46) Tomić, M.; Valentí, R.; Jeschke, H. O. *Phys. Rev. B* **2012**, *85*, 094105.
(47) Huhnt, C.; Michels, G.; Roepke, M.; Schlabitz, W.; Wurth, A.; Johrendt, D.; Mewis, A. *Physica B* **1997**, *240*, 26−37.
(48) Brüning, E. M.; Krellner, C.; Baenitz, M.; Jesche, A.; Steglich, F.; Geibel, C. *Phys. Rev. Lett.* **2008**, *101*, 117206.
(49) Kamihara, Y.; Hiramatsu, H.; Hirano, M.; Kawamura, R.; Yanagi, H.; Kamiya, T.; Hosono, H. *J. Am. Chem. Soc.* **2006**, *128*, 10012−10013.
(50) Hamlin, J. J.; Baumbach, R. E.; Zocco, D. A.; Sayles, T. A.; Maple, M. B. *J. Phys.: Condens. Matter* **2008**, *20*, 365220.
(51) Kamihara, Y.; Hiramatsu, H.; Hirano, M.; Kobayashi, Y.; Kitao, S.; Higashitaniguchi, S.; Yoda, Y.; Seto, M.; Hosono, H. *Phys. Rev. B* **2008**, *78*, 184512.
(52) Baumbach, R. E.; Hamlin, J. J.; Shu, L.; Zocco, D. A.; Crisosto, N. M.; Maple, M. B. *New J. Phys.* **2009**, *11*, 025018.
(53) Baumbach, R. E.; Hamlin, J. J.; Ho, P.-C.; Lum, I. K.; Maple, M. B. *Phys. Rev. B* **2012**, *85*, 104526.